Electronic Supplementary Information (ESI)

Intercalating a potassium-aqua complex cation into an α-MoO₃ layer without reducing molybdenum: a potential storage system†

Debu Jana, Shalini Sanjay Mishra and Samar K. Das*

School of Chemistry, University of Hyderabad, P.O. Central University, Hyderabad – 500046, India

Contents

Section S1. Experimental Section:

Materials. The chemicals, sodium molybdate ($Na_2MoO_4 \cdot 2H_2O$, SRL, extra-pure AR, 99%), cobalt chloride ($CoCl_2 \cdot 6H_2O$, SRL, extra-pure AR, 99%), glacial acetic acid (CH_3COOH, FINAR, extra-pure, 99.5%), potassium chloride (KCl, SRL, extra-pure AR, 99%), hydrochloric acid (HCl, FINAR, extra-pure, 99.5%) and distilled water are used for the synthesis of compound $[Mo^{VI}_4O_{12}(CH_3COO)_2\{Co^{II}(H_2O)_6\}]\cdot 2H_2O$ (**1**) and $[Mo^{VI}_3O_9\{K(H_2O)_4\}(CH_3COO)]\cdot H_2O$ (**2**). For electrochemistry, potassium chloride (KCl, extra-pure, Sigma Aldrich), sodium chloride (NaCl, extra-pure, Sigma Aldrich), carbon black powder (Sigma Aldrich), poly(vinylidene fluoride) (BLD Pharmatech, India), N-Methyl-2-pyrrolidone (SRL, 99.5% pure) and milli-q water have been used. The electrodes, carbon paper, graphite rod (diameter: 10 mm) and Hg/Hg_2Cl_2 (3M KCl) are purchased from the Sinsil Int. Pvt. Limited (India).

Synthesis of compound $[Mo^{VI}_4O_{12}(CH_3COO)_2\{Co^{II}(H_2O)_6\}]\cdot 2H_2O$ (1)[1]

10.0 ml of CH_3COOH (99.5%) was added to 10.0 ml aqueous solution of $Na_2MoO_4.2H_2O$ (2.0 g, 8.27 mmol). After stirring for 5 min, 5 ml solution of $CoCl_2.6H_2O$ (492 mg, 2.07 mmol) was added into it. After 10 min, the resulting solution was acidified with 12N HCl (1 ml) giving rise to a pH value of 2.3. It was filtered and the clear solution was kept for 2 weeks at room temperature. Pink crystals, precipitated from the solution during this time, were collected by filtration, washed with cold water and dried in air.

Synthesis of compound $[Mo^{VI}_3O_9\{K(H_2O)_4\}(CH_3COO)]\cdot H_2O$ (2)

As synthesized compound $[Mo^{VI}_4O_{12}(CH_3COO)_2\{Co^{II}(H_2O)_6\}]\cdot 2H_2O$ (**1**) (500 mg, 0.561 mmol) was added into a 50 ml of distilled water and it was allowed to stir for 30 min. The resulting solution was filtered to get clear solution of compound **1**. A 10 ml solution of KCl (1g, 13.51 mmol) was then added into the pink colored filtrated solution. The resulting solution mixture was stirred for 10 min more. Then it was kept for crystallization for 2 days at room temperature (25^0C). A white precipitate was observed after 2 days. The white product, $[Mo^{VI}_3O_9\{K(H_2O)_4\}(CH_3COO)]\cdot H_2O$ (**2**) was collected by filtration followed by washing with water for several times (5 times). Then, the filtered product was dried at room temperature for 24h. Yield: 74% based on Mo. IR data (cm^{-1}): 780 (Mo-O-Mo stretching), 891 (Mo=O stretching), 1471 (CH_3COO stretching), 1646 (H_2O bending), 3277 (O-H stretching); Raman data (cm^{-1}): 945

(Mo=O stretching), 912 (Mo-O-Mo stretching), 604 (K-O stretching), 375-213 (MoO_3 bending). Obsd. ICP-OES data: Mo (46.55%), K (6.38%); Carbon analysis: C (3.49%); TGA: water contents (13.1%), acetate content (9.41%); calculated data: Mo (46.42%), K (6.31%), C (3.87%), water contents (14.52%), acetate content (9.69%).

Characterization methods: We have recorded IR data of compounds **1** and **2** using iD7 ATR thermo Fisher Scientific-Nicolet iS5 instrument. All the PXRD data of this work were collected from Bruker D8 Advance diffractometer using graphite monochromated Cu Kα1 (1.5406 A) and Kα2 (1.54439 A) radiation. A Wi-Tec alpha 300AR laser confocal optical microscope (T-LCM) facility equipped with a Peltier-cooled CCD detector was used to record the Raman data of compounds **1** and **2** using a 683 nm argon ion laser. Thermogravimetric analysis (TGA) of compound **2** was performed on a STA 409 PC analyzer. Solid state UV-visible studies of compounds **1** and **2** were carried out using UV- 2600 Shimadzu UV−visible spectrometer in the diffuse reflectance mode. Carl Zeiss model Ultra 55 microscope instrument was used for field emission scanning electron microscope (FESEM) imaging and energy dispersive X-ray (EDX) analysis.

Electrochemical measurements:

All the electrochemical studies (cyclic voltammetry) were carried out using a conventional three electrodes system, where carbon paper (coated by compound **2**), Hg/Hg_2Cl_2 (3 M KCl) and graphite rod (diameter: 10 mm) were used as working electrode, reference electrode and counter electrodes, respectively. Galvanostatic charge/discharge studies were performed using two electrode system, where carbon paper (coated by compound **2**) and graphite rod were used as cathode and anode, respectively. The working electrode material was prepared by mixing compound $[Mo^{VI}_3O_9\{K(H_2O)_4\}(CH_3COO)]\cdot H_2O$ (**2**) (powder form), carbon black, poly(vinylidene fluoride) (PVDF) at a weight ratio of 8:1:1. Then slurry was prepared using N-Methyl-2-pyrrolidone (NMP) solvent. The active material was coated on the carbon paper working electrode of 1 mg/cm^2 loading. The prepared coated working electrodes were allowed to dry at 60 ^{0}C for 24 h. All electrochemical measurements and aqueous storage application were performed using CHI-6057E instrument. The electrolytes were 0.5 M KCl and 0.5 M NaCl (pH 2.0).

Section S2. Characterization of compound 2:

Section S2.1. IR analysis:

Fig. S1a represents the full range IR spectrum of compound **2**. We have also compared the IR spectra of both compounds **2** and **1** as shown in Fig. S1b. The peaks for the stretching vibration for the MoO$_3$ moiety are almost similar for both compounds **2** and **1** as shown in Fig. S1c.
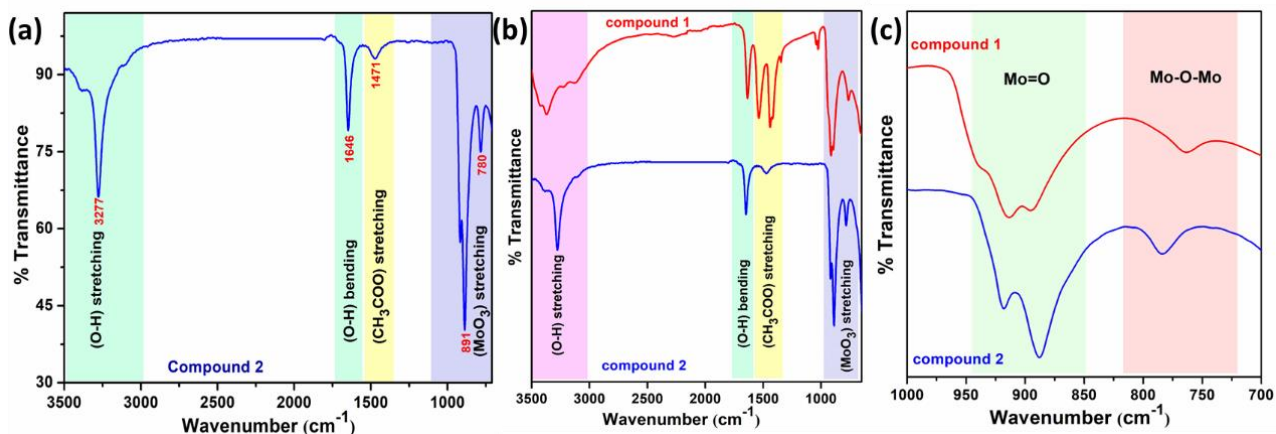
Fig. S1. (a) IR spectrum of compound **2**; (b)-(c) IR spectra comparison plots of compounds **2** and **1**.

Section S2.2. UV-visible studies:

In this work, we have synthesized compound [Mo$^{VI}_3$O$_9$\{K(H$_2$O)$_4$\}(CH$_3$COO)]·H$_2$O (**2**) by intercalating K-aqua complex into interlamellar space of α-MoO$_3$ of compound [Mo$^{VI}_4$O$_{12}$(CH$_3$COO)$_2$\{Co^{II}(H$_2$O)$_6$\}]·2H$_2$O (**1**) by replacing Co-hexa-aqua complex. As shown in Fig. S2, the UV-visible spectrum of compound **1** shows clear absorbance peaks in visible region (wavelength: 400-700 nm) due the d-d transition of Co(II) center, whereas compound **2** does not show any absorbance peaks in same visible region due to absence of Co(II) center (all the Co(II) centers are replaced by K(I) centers) and K(I) centers cannot exhibit any absorbance peak in visible region.
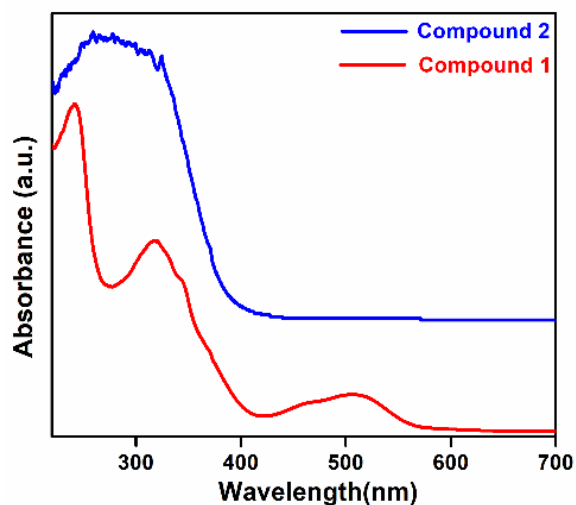
Fig. S2. UV-visible spectra of compounds **2** and **1**.

Section S2.3. XPS analysis:

Generally, in XPS analysis of a molybdenum bronze, Mo 3d5/2 shows a major contributor peak at 232.1 eV and a minor contributor peak at 233.0 eV, which are due to Mo^{6+} and Mo^{5+}, respectively. Likewise, Mo 3d3/2 shows a major contributor peak at 235.3 eV and a minor contributor peak at 236.3 eV, which are due to Mo^{6+} and Mo^{5+}, respectively.[2] The XPS spectrum of compound **2** indicates the presence of molybdenum, potassium, oxygen and carbon as shown in Fig. S3b. However, the XPS plot of compound **2** shows only two major contributor peaks at 232.5 and 235.6 eV, that correspond to Mo 3d5/2 and Mo 3d3/2 of Mo^{6+}, respectively as shown in Fig. S3a.
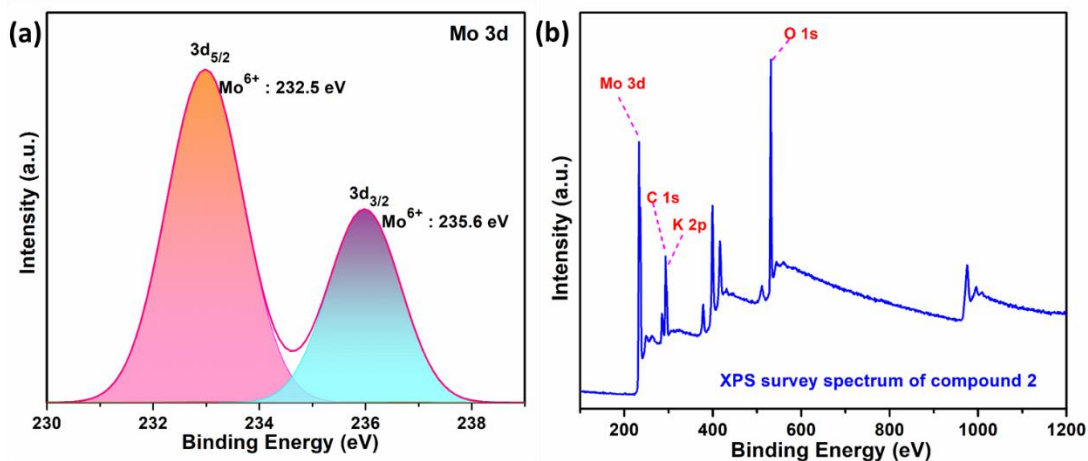
Fig. S3. (a) XPS plot of the Mo 3d core level in compound **2**; (b) XPS survey spectrum of compound **2**.

Section S2.4. Energy dispersive X-ray (EDX) and mapping analyses:
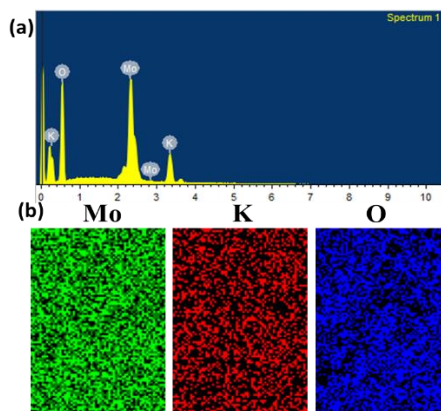
Fig. S4. (a) Energy dispersive X-ray (EDX) histogram of compound **2**; (b) elemental mapping analysis of compound **2**.

Section S2.5. ICP-OES and carbon analyses:

The ICP-OES analysis (a quantitative analysis) of compound $[Mo^{VI}_3O_9\{K(H_2O)_4\}(CH_3COO)]\cdot H_2O$ (**2**) indicates the presence of Mo (46.55%) and K (6.38%) as shown in Table S1 (ESI). The carbon analysis of compound **2** confirms the presence and C-quantity (3.49%) as shown in Table S2 (ESI). Based on the ICP-OES and carbon analysis data, we have determined the formula of compound **2** as $[Mo^{VI}_3O_9\{K(H_2O)_4\}(CH_3COO)]\cdot H_2O$, which closely matches the calculated mass percentage of Mo (46.42%), K(6.31%) and C(3.87%).

Table S1. ICP-OES analysis of compound **2**.

Elements	ICP-OES mass %	Calculated mass %
Molybdenum (Mo)	46.55	46.42
Potassium (K)	6.38	6.31

Table S2. Carbon analysis of compound **2**.

Elements	Carbon analysis mass %	Calculated mass %
Carbon (C)	3.49	3.87

Section S2.6. Thermogravimetric analysis (TGA):

TGA analysis of compound $[Mo^{VI}_3O_9\{K(H_2O)_4\}(CH_3COO)]\cdot H_2O$ (**2**) shows two successive weight losses, where first weight loss of 13.1% (calculated: 14.52%) is due to water molecules loss and another weight loss of 9.41% (calculated: 9.69%) is due to CH_3COO group loss (Fig. S5). The total water content and CH_3COO content in compound **2** are also consistent with TGA analysis of compound **2** as shown in Table S3.
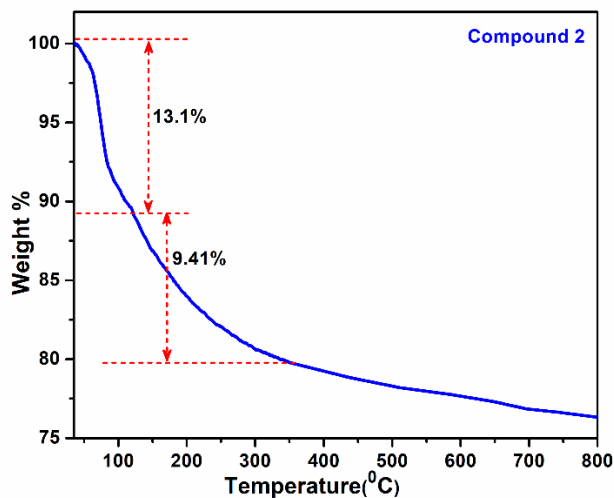
Fig. S5. TGA plot of compound **2**.

Table S3. Data analysis of TGA plot of compound **2**.

Components	Theoretical wt% from formula of compound 2	Experimental wt% from TGA plot
Water (H_2O)	14.52	13.10
Acetic acid (CH_3COOH)	9.69	9.41

S8

Section S2.7. About CH₃COO⁻ anion in compounds 1 and 2:

It is important to mention that in parent compound **1**, the acetate anion (CH_3COO^-) is coordinated to the Mo(VI) centre of α-MoO_3 layers, which we could characterize by single crystal X-ray crystallography and formulate the compound as $[Mo^{VI}_4O_{12}(CH_3COO)_2\{Co^{II}(H_2O)_6\}]\cdot 2H_2O$ (**1**) (Fig. S6a). On the other hand, compound **2**, which we could not characterize by single crystal X-ray crystallography, but we could thoroughly characterize by extensive spectral analyses including ICP metal analysis, includes non-coordinated acetate anion as an intercalant with potassium-aqua complex cation, forming a salt kind of species in the inter-lamellar space, as suggested by IR spectral- and XPS-analyses. As shown in the IR spectra, shown in Fig. S1b, the stretching vibration of CH_3COO^- group of compound **2** is quite different than that of compound **1**. This preliminarily indicates that the bonding fashion of CH_3COO^- anion of compound **2** is different than that in compound **1**. As shown in the IR spectrum of compound **2** (Fig. S1b), the acetate peak became smaller in intensity and gets slightly shifted towards high energy region (it is a tiny shift if one carefully / closely look at it). This clearly indicates that acetate anion is not coordinated to Mo(VI) centers of MoO_3 layers unlike that in compound **1**; the coordination of acetate anion to Mo(VI) center in compound **1** causes lowering of electron density of COO^- group and thereby results in COO^- peak shift towards lower energy side. So, little high-energy (or high cm⁻¹) shift of the COO^- peak in the IR spectrum of compound **2** indicates that acetate anion is not coordinated to Mo(VI) center (of MoO_3 layers) in compound **2**. We have thus proposed that in compound $[Mo^{VI}_3O_9\{K(H_2O)_4\}(CH_3COO)]\cdot H_2O$ (**2**), acetate anions are present into the α-MoO_3 layers as an intercalant with potassium-aqua complex cation as $[K(H_2O)_4][OCOCH_3]$ salt-like species with some sort of associated distance between $[K(H_2O)_4]^+$ and $[OCOCH_3]^-$. Moreover, the fitted C 1s XPS plots for CH_3COO^- group of compound **2** is quite different than that of compound **1** as shown in Fig. S6b-c. In the C 1s XPS plot of compound **2**, the binding energy value at 285.16 eV corresponds to the presence of potassium-acetate salt.
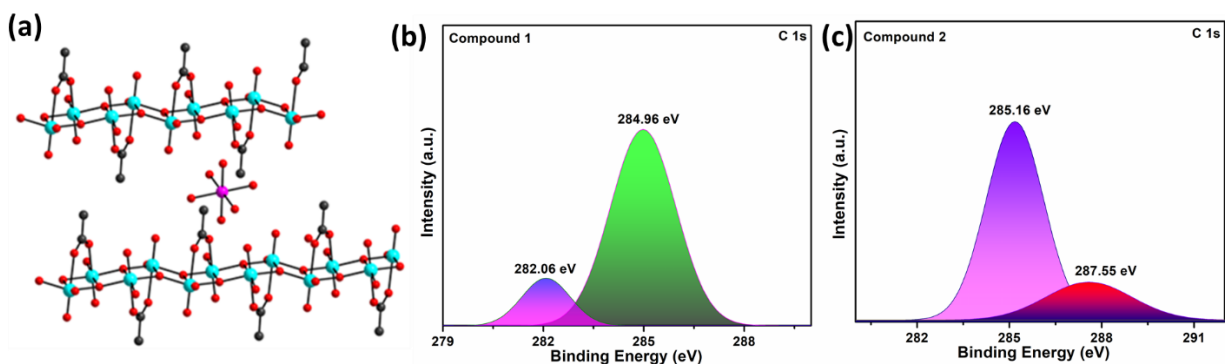
Fig. S6. (a) Intercalation of cobalt-hexa-aqua complex cation, $[Co^{II}(OH_2)_6]^{2+}$ in between MoO_3 layers with acetate coordination to the MoO_3-layer as found in the crystal structure of compound **1**. Color code: Mo, cyan; Co, pink; O, red; C, dark gray; (b) XPS plot of C 1s level of compound **1**; (c) XPS plot of C 1s level of compound **2**.

Section S2.8. Evidences of Intercalation of K⁺ cation into α-MoO₃ layer:
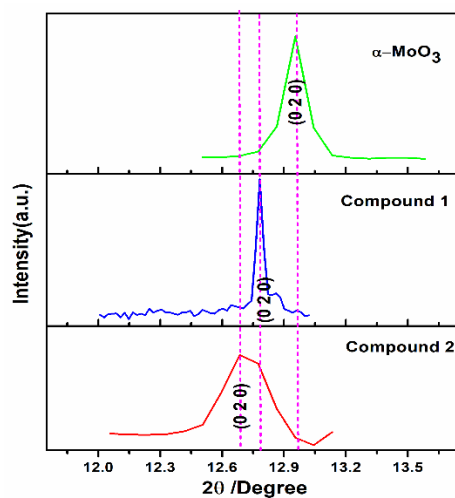
Fig. S7. PXRD peak (0 2 0) of compound **2** (red line), compound **1** (blue line) and α-MoO₃ (green line).
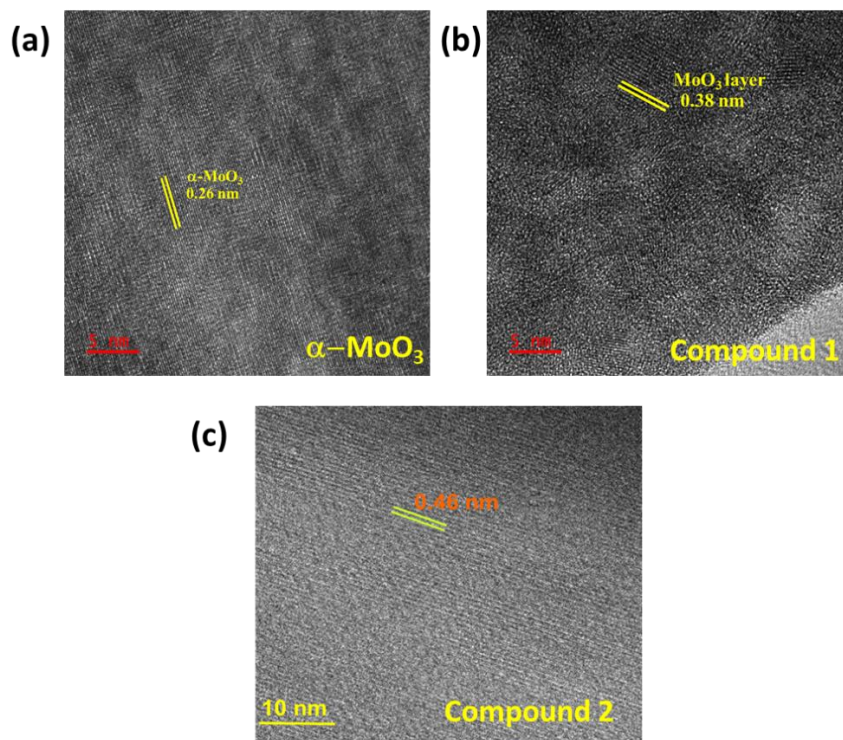
Fig. S8. (a) HRTEM image of α-MoO₃ (commercial), showing its fringe gap of 0.26 nm; (b) HRTEM image of compound **1**, showing its fringe gap of 0.38 nm; (c) HRTEM image of compound **2**, showing its fringe gap of 0.46 nm.

Section S3. Electrochemistry and storage applications:

Section S3.1. Schematic representation of the overall reaction process in CV

$[Mo^{VI}_3O_9\{K(H_2O)_4\}(CH_3COO)]$

$2e^-, 2K^+$
Charging
K^+ extraction

$2e^-, 2K^+$
Discharging
K^+ insertion

$K_2[Mo^{VI}Mo^V_2O_9\{K(H_2O)_4\}(CH_3COO)]$
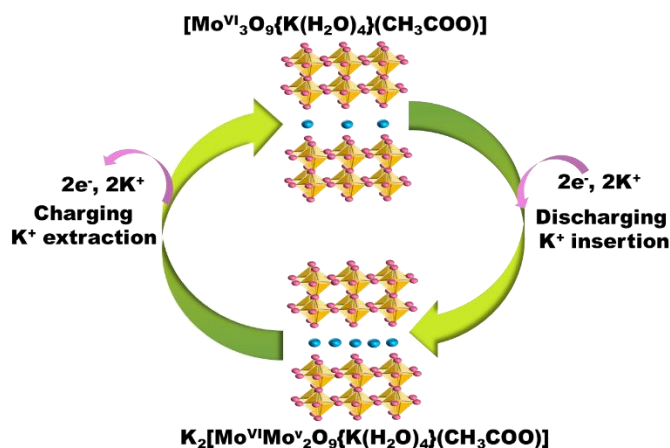
Scheme S1. Schematic diagram for charging and discharging processes of compound **2**, showing extraction and insertion of K^+ cation, respectively.

Section S3.2. Electrochemical impedance spectroscopy (EIS):
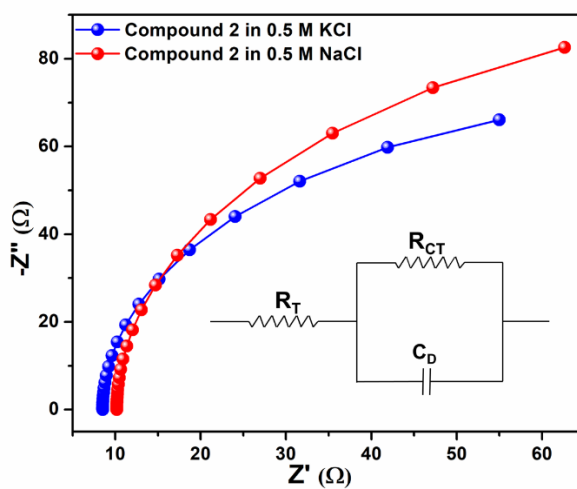
Fig. S9. Electrochemical impedance plots of compound **2** (coated on carbon paper) in 0.5 M KCl (blue line) and 0.5 M NaCl (red line) electrolytes.

Section S3.3. Electrochemical reaction kinetics and mechanism:
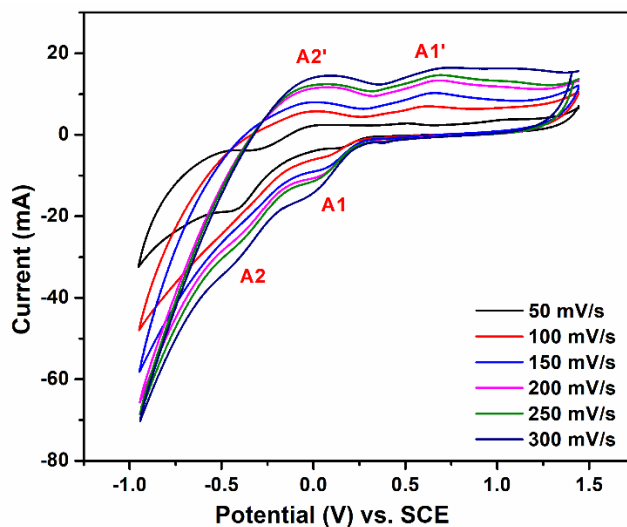
Fig. S10. CV plots of compound **2** in 0.5 M KCl electrolyte at various scan rates.
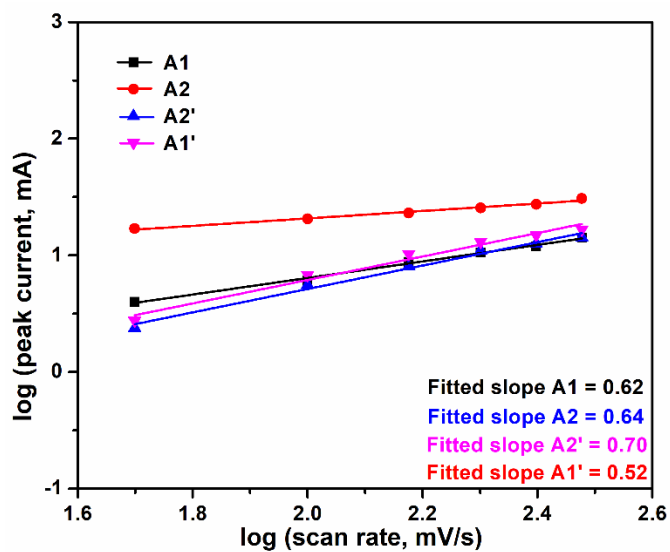
Fig. S11. Plot of log (scan rate) *versus* log (peak current) of compound **2** in 0.5 M KCl electrolyte; plots of log(*v*) *vs.* log(*i*).
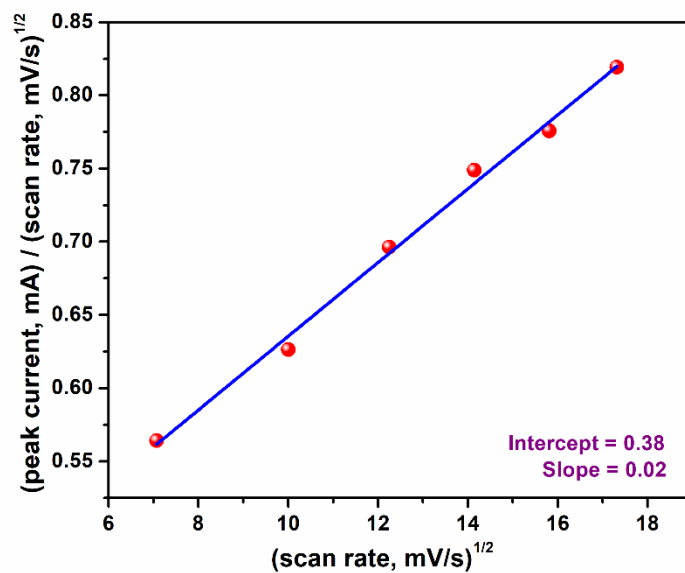
Fig. S12. Plot of (scan rate)$^{1/2}$ *versus* (peak current/scan rate)$^{1/2}$: plot of $v^{1/2}$ *vs* $(i(v)/v)^{1/2}$.
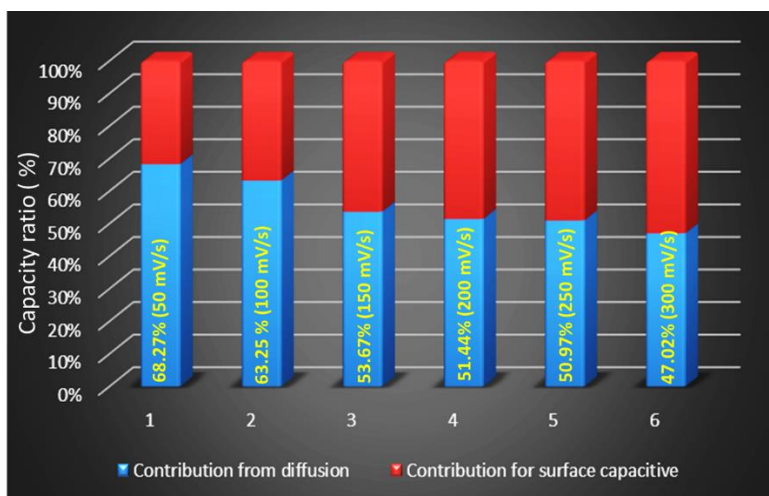
Fig. S13. Histograms for comparison of the capacity ratio of compound **2** in 0.5 M KCl electrolyte at 50-300 mV/s scan rates.

Table S4. Literature survey of MoO_3 based materials for storage application.

Materials	Electrolyte	Capacity (mA h g^{-1})	Current density (mA g^{-1})	References
Hexagonal MoO_3 nanorod	1 M $AlCl_3$	300	3000	3
h-MoO_3	1 M $ZnSO_4$	120	200	4
K_xMoO_3@C	1 M $LiPF_6$	258	118	5
α-MoO_3 Nanoparticles	$Ca(TFSI)_2$	165	20	6
MoO_3−$CoMoO_4$ microspheres	1 M $LiPF_6$	155.7	100	7
$Ca_{0.13}MoO_3 \cdot (H_2O)_{0.41}$	0.5 M $Ca(ClO_4)_2$	192	86	8
$[Mo^{VI}_3O_9(CH_3COO)\{K(H_2O)_4\}] \cdot H_2O$ (2)	0.5 M KCl	214	350	**This work**

Section S3.4. Storage application:
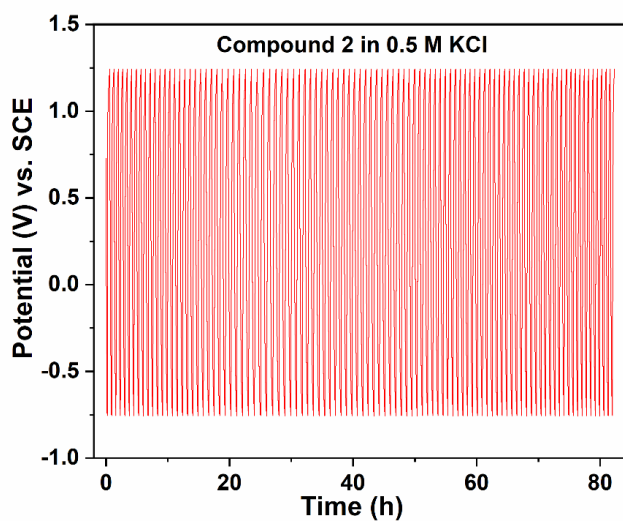
Fig. S14. Time *versus* potential plot of compound **2** in 0.5 M KCl electrolyte, obtained from charge-discharge cycling.
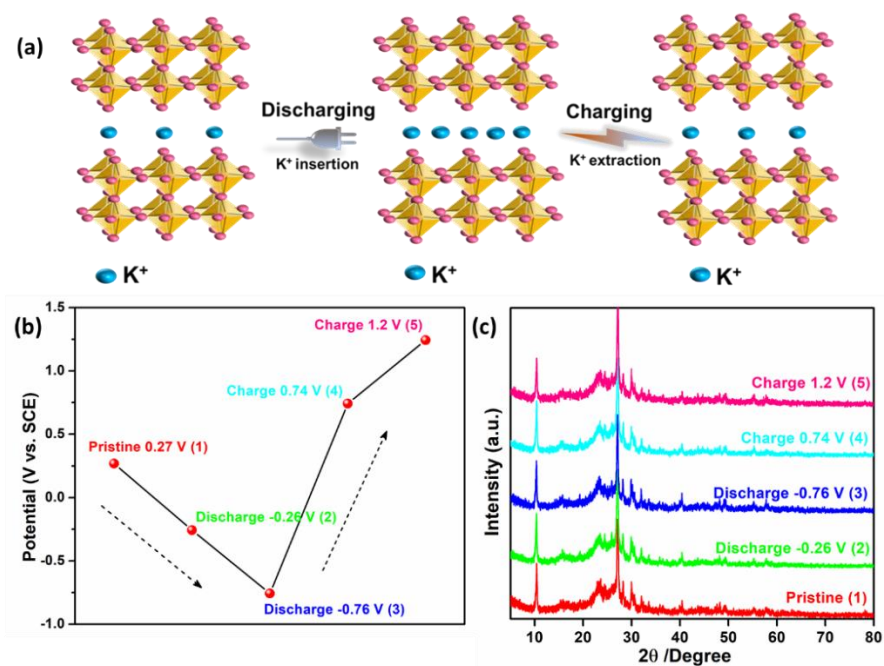
Fig. S15. (a) Indication of K$^+$ intercalation during discharging process and K$^+$ deintercalation during charging process; (b) indication of different charge and discharge states; (c) PXRD patterns of compound **2** at different charge and discharge states.
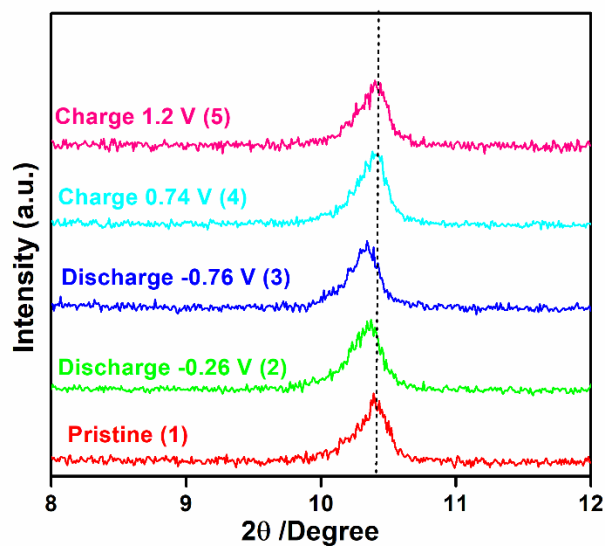
Fig. S16. PXRD patterns of compound **2**, indicating (0 2 0) at different charge and discharge states.
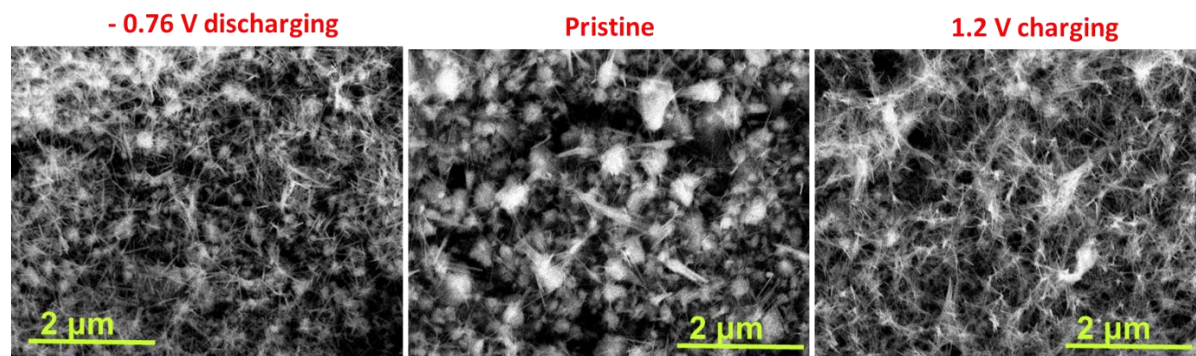
Fig. S17. FESEM images of compound **2** at different charge and discharge states.
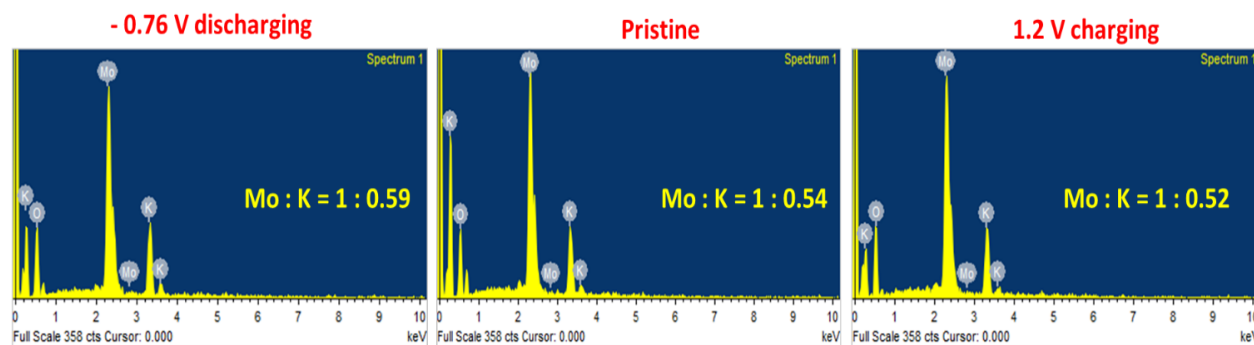
Fig. S18. EDX histograms of compound **2** at different charge and discharge states.
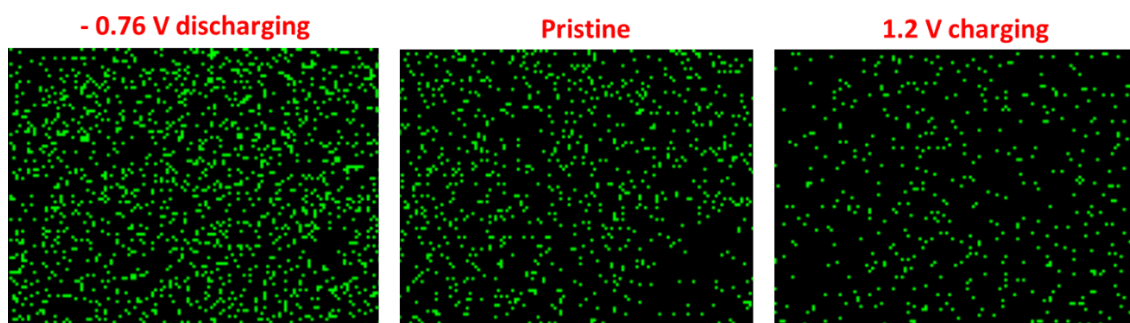
Fig. S19. EDX-elemental mapping of potassium (K) in compound **2** at different charge and discharge states.
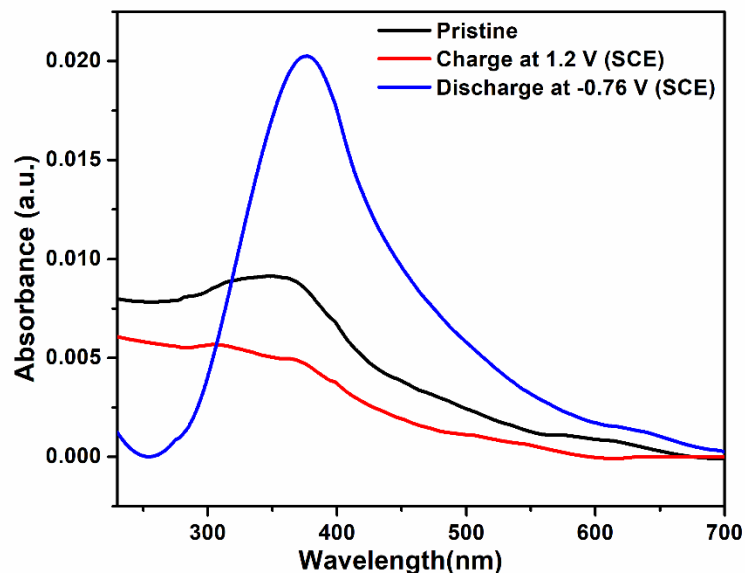
Fig. S20. UV-visible spectra of compound **2** at different charge and discharge states.

References

1. D. Jana, H. K. Kolli, and S. K. Das, *Chem. Mater.,* 2023, **35**, 3083−3094.

2. F. Xie, W. C. H. Choy, C. Wang, X. Li, S. Zhang, J. Hou, *Adv. Mater.,* 2013, **25**, 2051−2055.

3. J. Joseph, A. P. O'Mullane and K. Ostrikov, *ChemElectroChem.,* 2019, **6**, 6002.

4. T. Xiong, Y. Zhang, Y. Wang, W. S. V. Lee and J. Xue, *J. Mater. Chem. A*, 2020, **8**, 9006–9012.

5. Z. Hu, X. Zhang, C. Peng, G. Lei, Z. Li, *Journal of Alloys and Compounds.,* 2020, **826**, 154055.

6. S. Kim, L. Yin, S. –M. Bak, T. T. Fister, H. Park, P. Parajuli, J. Gim, Z. Yang, R. F. Klie, P. Zapol, Y. Du, S. H. Lapidus, and J. T. Vaughey, *Nano Lett*., 2022, **22**, 2228−2235.

7. W. Wang, J. Qin, Z. Yin, and M. Cao, *ACS Nano*, 2016, **10**, 10106−10116.

8. M. S. Chae, H. H. Kwak and S. –T. Hong, *ACS Appl. Energy Mater*., 2020, **3**, 5107−5112.

****